



ELSEVIER

Available online at [www.sciencedirect.com](http://www.sciencedirect.com)
**jmr&t**  
 Journal of Materials Research and Technology
journal homepage: [www.elsevier.com/locate/jmrt](http://www.elsevier.com/locate/jmrt)**Original Article**

# Structural, thermal, and mechanical investigation of telluro-borate-Bismuth glass for radiation shielding

Hammam Abdurabu Thabit <sup>a,\*</sup>, Abd Khamim Ismail <sup>a</sup>, Hicham Es-soufi <sup>b</sup>, D.A. Abdulmalik <sup>c</sup>, Abdo Mohammed Al-Fakih <sup>d</sup>, Shoroog Alraddadi <sup>e</sup>, M.I. Sayyed <sup>f,g</sup>

<sup>a</sup> Department of Physics, Universiti Teknologi Malaysia, 81310, Johor Bahru, Malaysia

<sup>b</sup> Laboratory of Sciences and Professions of the Engineer, Materials and Processes Department ENSAM-Meknes Marjane II, Moulay Ismail University, El Mansour, Meknes P.O. Box 15290, Morocco

<sup>c</sup> Department of Mathematics, Statistics and Physics, College of Arts and Sciences, Qatar University, 2713, Doha, Qatar

<sup>d</sup> Department of Chemistry, Faculty of Science, Universiti Teknologi Malaysia, Johor, Malaysia

<sup>e</sup> Department of Physics, Umm AL-Qura University, Makkah, Saudi Arabia

<sup>f</sup> Department of Physics, Faculty of Science, Isra University, Amman 11622, Jordan

<sup>g</sup> Department of Nuclear Medicine Research, Institute for Research and Medical Consultations, Imam Abdulrahman bin Faisal University, Dammam 31441, Saudi Arabia

**ARTICLE INFO****Article history:**

Received 8 February 2023

Accepted 10 April 2023

Available online 12 April 2023

**Keywords:**

Boro-tellurite glass

Hardness

DTA

Radiation shielding

**ABSTRACT**

The radiation shielding properties of telluro-borate glasses have a great importance in nuclear industry. This work focused on the study of the glasses of the  $(70-x)\text{B}_2\text{O}_3-5\text{TeO}_2-20\text{SrO}-5\text{ZnO}-x\text{Bi}_2\text{O}_3$  (with  $0 \leq x \leq 15\% \text{ mol}\%$ ) system, which have been synthesized by the melt-quenching route. The scanning electron microscope (SEM) analysis showed no agglomeration on glassy surfaces, which confirmed the amorphous state. The thermal differential analysis (DTA) showed that the glass transition temperature ( $T_g$ ) decreased from 589.90 °C to 529.51 °C with replacing  $\text{B}_2\text{O}_3$  mol% by  $\text{Bi}_2\text{O}_3$  mol%. The mechanical properties of these glasses have been evaluated by investigation of the parameters, such as the bulk modulus ( $K$ ), the Young's modulus ( $E$ ), the shear modulus ( $S$ ), the longitudinal modulus ( $L$ ), and the Poisson coefficient, which are changed by  $\text{Bi}_2\text{O}_3$  doping. The radiation shielding properties of these prepared glasses have been evaluated, and we reported the effective atomic number ( $Z_{\text{eff}}$ ) at 0.511 MeV. The results showed that the glass with  $x = 15\%$  has the highest  $Z_{\text{eff}}$ . We found that the  $Z_{\text{eff}}$  is almost doubled when the concentration of  $\text{Bi}_2\text{O}_3$  is increased from 0 mol% to 15 mol%. The findings provide a deeper understanding of the thermal, mechanical, and shielding properties of glass and have potential applications in areas such as construction and radiation protection.

© 2023 The Author(s). Published by Elsevier B.V. This is an open access article under the CC BY-NC-ND license (<http://creativecommons.org/licenses/by-nc-nd/4.0/>).

\* Corresponding author.

E-mail addresses: [hammam.tha@gmail.com](mailto:hammam.tha@gmail.com), [a.abdurabu@utm.my](mailto:a.abdurabu@utm.my) (H.A. Thabit).

<https://doi.org/10.1016/j.jmrt.2023.04.082>

2238-7854/© 2023 The Author(s). Published by Elsevier B.V. This is an open access article under the CC BY-NC-ND license (<http://creativecommons.org/licenses/by-nc-nd/4.0/>).

## 1. Introduction

Glass is a material that is frequently used for the purposes of radiation shielding, and scientists are constantly looking into new methods for producing glasses that are more efficient [1]. In this regard, due to their great density and efficiency at absorbing gamma photons, lead-based glasses are presently the most frequently employed materials for radiation protection [2,3]. However, research and development efforts are currently underway to design and test novel materials that have the potential to increase shielding effectiveness while also reducing weight. These advancements are essential for enhancing the protection and safety of personnel who are subjected to ionizing radiation in a variety of different sectors [4–8]. Glass is an essential component in the development of a wide variety of new technologies, due to the fact that it possesses a rare combination of qualities, such as durability, transparency, and a low cost of production. Optical fiber communication, solar panels, touchscreens, the automobile sector, architecture, healthcare, radiation protection, and the production of energy are some examples of applications for glasses [9–14]. Glass's thermal characteristics, such as its glass transition temperature, crystallization temperature, and melting temperature, are key factors in influencing the effectiveness, safety, and efficiency of glass applications and products. These characteristics are important for comprehending the behavior patterns of glass products under different thermal and environmental factors in addition to their design, optimization, and processing. Investigating the thermal properties of glasses can open up new possibilities for their usage in a variety of applications and support the development of innovative glass-based products [15–19].

On the other hand, the durability and dependability of glass products in a variety of applications are significantly influenced by the mechanical properties of glass, notably their elastic moduli and hardness. The shaping, cutting, and polishing of glass all depend on the mechanical qualities of the glass being processed, and these properties play a significant role. Knowing about these characteristics can assist in improving the quality of glass products as well as the requirements under which they are processed by optimizing the conditions [20–22].

The analysis of the thermal, structural, and mechanical properties of radiation shielding glasses can provide extremely helpful insight and understanding into the behavior and capabilities of these materials under a wide variety of different situations. With the use of this knowledge, radiation shielding glass processes can be made more efficient, safety and dependability can be ensured, and new and better radiation protection products can be developed for a range of applications [23–27].

In this paper, we prepare new borate glasses with different concentrations of  $\text{Bi}_2\text{O}_3$ . The addition of  $\text{Bi}_2\text{O}_3$  to borate glasses has a number of advantages, including greater thermal stability, increased radiation shielding, and enhanced mechanical characteristics, making it a crucial component in many applications. When it comes to radiation shielding applications,  $\text{Bi}_2\text{O}_3$  is chosen over  $\text{PbO}$  due to the fact that it is less

hazardous, has a higher density, is cost-effective, is readily available, and is less harmful to the environment. In comparison to  $\text{PbO}$ , the substance  $\text{Bi}_2\text{O}_3$  has a lower impact on the surrounding environment.

## 2. Materials and methods

### 2.1. Glass preparation

By using the melt quenching approach, a number of glasses with formulas  $(70-x)\text{B}_2\text{O}_3-5\text{TeO}_2-20\text{SrO}-5\text{ZnO}-x\text{Bi}_2\text{O}_3$ ,  $x = 0\%, 1\%, 5\%, 10\%$ , and  $15\%$  mol have been obtained, as explained in previous studies [28]. S1, S2, S3, S4, and S5 were the designations given to the created glasses for  $x = 0, 1, 5, 10$ , and  $15$  mol% of  $\text{Bi}_2\text{O}_3$ . Using the classic Archimedes method and toluene as the liquid medium, the density ( $\rho$ ) of the produced glass specimens was computed as shown in Table 1.

**Table 1 – Density and physical image for the glass samples.**

Sample code	Density (g/cm <sup>3</sup> )	The physical image
S1	2.90	
S2	3.00	
S3	3.41	
S4	3.92	
S5	4.28	

## 2.2. Morphology study

With the aid of an energy dispersive X-ray spectroscopy (EDX) analyzer-equipped scanning electron microscope (SEM), all of the prepared glasses were examined. The EDX allows for an approximate estimation of the elemental elements contained in the examined glasses. A 5.00 kV electron beam was used to acquire the microstructures at a magnification of 10 kV.

## 2.3. The differential thermal analysis DTA

The differential thermal analysis DTA is a critical technique for glassy materials, as it indicates the temperature at which the material transitions from a rigid, glassy state to a flexible, rubbery state, which enables us to understand the underlying thermal transition processes. In this regard, the DTA discloses more information on the thermal stability of glass during the manufacturing process and identifies potential issues such as defects, impurities, or variations in composition that can affect the thermal properties, including heat capacity, enthalpy, and temperature dependence of the thermal transitions. This information can be used to understand the underlying mechanisms of thermal transitions and optimize the processing and performance of glass materials. The PerkinElmer and Pyris Diamond (TG/DTA) instrument was used to perform a differential thermal analysis to determine the glass transition temperature  $T_g$ . In this experiment, 20 mg of the powdered glass sample was heated in a platinum pan at a rate of 10 °C per minute between 30 and 1000 °C.

## 2.4. Mechanical properties

Mechanical testing helps to ensure that the glass produced meets the required specifications and standards for strength and durability. Due to the use of glass in various applications such as building construction, automotive, and consumer goods. Testing the mechanical properties helps to ensure that the glass will not fail under normal conditions and will not pose a safety risk to people and property. In this regard, by understanding the mechanical properties of glass, engineers can optimize the design of glass components and structures, improving their performance and reliability. For example, the hardness test can determine its resistance to scratching, abrasion, and other forms of surface damage. Testing the hardness of glass helps to ensure that it will retain its appearance and functionality over time. For a specific purpose, such as radiation protection or optical components, we need glass materials, which depend on the hardness of these materials. Moreover, calculating the elastic modulus is necessary to determine how hard glass samples are.

Herein, a suitable method of studying mechanical properties of small volume materials is via indentation hardness, where a fixed load on the diamond indenter is applied and measured using a microscope. Vickers hardness is the most widely used among several geometry indenters in hardness testing. The diamond pyramid hardness number  $H_V$  is the ratio of the applied load ( $P$ ) to the contact surface area ( $a^2$ ) (see Eq. (1)). Low load hardness testing was conducted and a load levels of 50 N with dwell period of 20s at room temperature [29].

$$H_V = \frac{P}{a_0 a^2} \quad (1)$$

Where  $a_0$  is an indenter constant of 2.157, the present experiment used a diamond pyramid indenter.

The period of pulse reception display was evaluated for longitudinal velocity ( $V_L$ ) and shear velocity ( $V_S$ ) [30].

This relation was used to obtain the ultrasonic velocity (see Eqs. (2) and (3)).

$$V_L = \frac{2d}{\Delta t} \quad (2)$$

$$V_S = \frac{2d}{\Delta t} \quad (3)$$

Where  $d$  is the glass thickness and  $\Delta t$  is the period gap.

The elastic modulus is expressed using Cauchy relation:

$$L = \rho V_L^2 \quad (4)$$

(L) denotes a homogeneous isotropic material.

$$G = \rho V_S^2 \quad (5)$$

G represents shear resistance.

Bulk modulus (K) represents hydrostatic pressure incompressibility.

$$K = 3L - 4G \quad (6)$$

Young modulus describes the uniaxial proportionality of stress and strain.

$$E = 2(1 + \sigma)G \quad (7)$$

The Poisson's ratio identifies the ratio of axial strain to radial strain [30].

$$\sigma = \frac{L - 2G}{2(L - G)} \quad (8)$$

Poisson's ratio  $\sigma$  was analyzed via Eq. (8).

## 3. Results and discussion

### 3.1. Scanning electron microscope (SEM) analysis

The prepared glasses, labelled S1, S2, and S5, are analyzed by scanning electron microscopy (SEM) to determine the surface morphology of the glasses. The obtained surface photographs by scanning electron microscopy (SEM) corresponding to the three glasses (S1, S2, and S5) are shown in Fig. 1(a–c). The SEM photographs show the surface morphology of the three glasses analyzed (S1: 1 μm, S2: 5 μm, and S5: 1 μm). From the comparison of the SEM photographs, the corresponding surfaces for these three glasses are characterized by smooth surfaces without any clusters [31,32]. So, these obtained SEM photographs conform to the amorphous state that was studied by X-ray diffraction patterns by exposing a broad peak of the studied glasses [28]. Furthermore, it observed similarities among all sample profiles. The bismuth oxide-doped glasses showed a similar morphology, too.

Fig. 1. SEM images of S1, S2 and S5 glass samples respectively.

### 3.1. B. energy-dispersive X-ray spectroscopy (EDX)

Energy-dispersive X-ray spectroscopy (EDX) is used to evaluate the concentrations of the elements present in the prepared glasses. Fig. 2(d-f) shows the X-ray spectra produced by

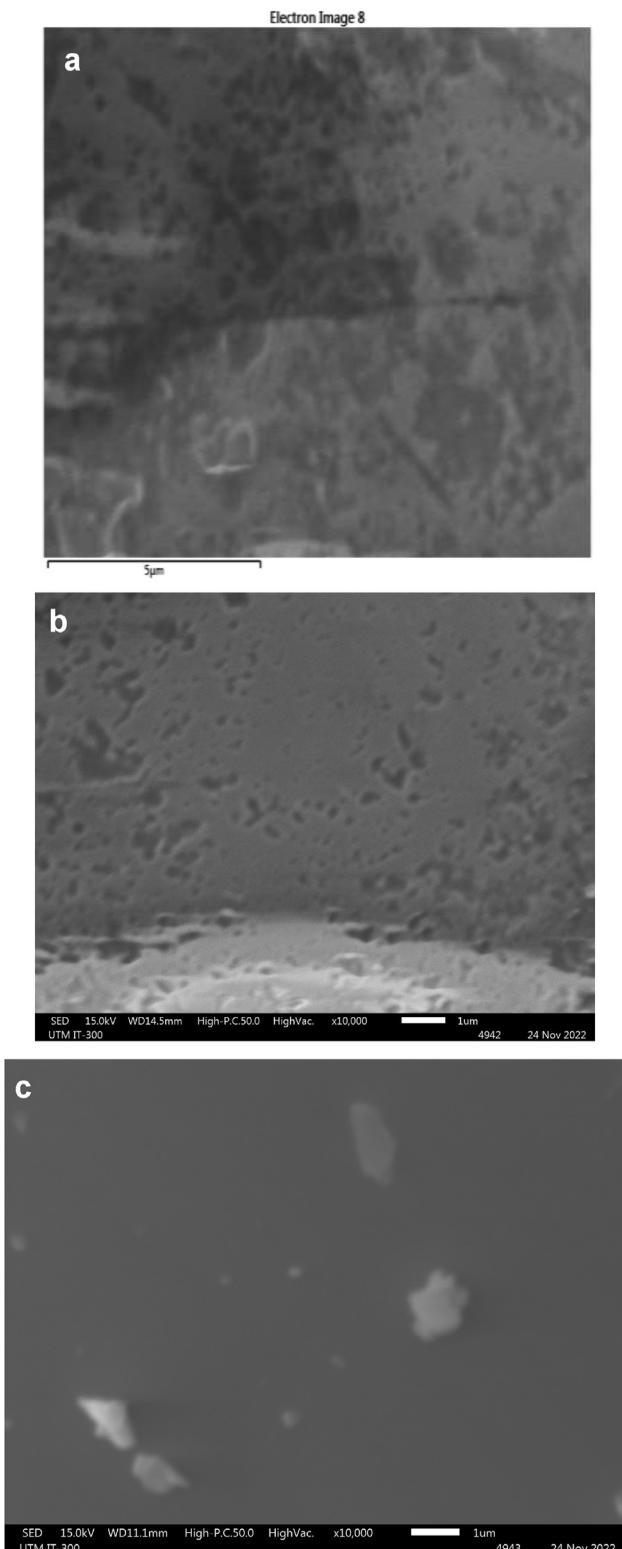


**Fig. 1 – SEM images of S1(a), S2(b) and S5(c) glass samples (please replace these SEM photo by other of glasses).**

the EDX analysis of the glasses S1(d), S2(e), and S5(f). From Fig. 2(d-f), it is observed that all EDX spectra reveal that the glasses are free from contamination since only the expected constituents are present (O, B, Bi, Te, Sr, and Zn). The atomic and weight data for several elements acquired from the EDX analyses are listed in Table 2. However, the intensity corresponding to each peak for each element in the EDX spectra changed from composition to composition, which means that the intensity of each element depends on its concentration [33,34].

### 3.2. Differential thermal analysis

The differential thermal analysis was investigated to study the prepared glasses of the  $(70-x)\text{B}_2\text{O}_3-5\text{TeO}_2-20\text{SrO}-5\text{ZnO}-x\text{Bi}_2\text{O}_3$  system, with ( $x = 0\%$  (S1), 1% (S2), 5% (S3), 10% (S4), and 15 mol% (S5)). Fig. 3 (S1–S5) shows the thermograms recorded in the temperature range 40–1000 °C, corresponding to the glasses S1 and S5. These thermograms depict three important parameters: glass transition temperature ( $T_g$ ), crystallization temperature ( $T_c$ ), and melting temperature ( $T_m$ ), which strongly depend on the chemical composition of the prepared glasses. Thanks to the evolution of the values corresponding to these parameters ( $T_g$ ,  $T_c$ , and  $T_m$ ) (see Table 3), it can study the influence of  $\text{Bi}_2\text{O}_3$  content replacing  $\text{B}_2\text{O}_3$  content in the glassy framework.  $T_g$  is slightly reduced from 589.90 °C (S1) to 529.51 °C (S5) when 1 mol%  $\text{Bi}_2\text{O}_3$  content is inserted into the glassy framework. It is widely known that the glass transition temperature is a structurally sensitive characteristic that depends on the bond strength, degree of cross-link density, and packing density [35]. Through the insertion of  $\text{Bi}_2\text{O}_3$  into the glass-network, the Bi–O bonds ( $\Delta H_f^{298} = 343 \text{ Kj/mol}$ ) replace B–O the bonds ( $\Delta H_f^{298} = 806 \text{ Kj/mol}$ ) [36]. It was expected that once  $\text{Bi}_2\text{O}_3$  replaced  $\text{B}_2\text{O}_3$ , the  $T_g$  would decrease, and the experimental data conformed to this expectation (see Fig. 4 and Table 3). In addition to the slight decreasing of the parameters, crystallization temperature ( $T_c$ ), and melting temperature ( $T_m$ ) went from 737.74 °C (S1) to 733.20 °C (S5) and from 895.05 °C (S1) to 862.56 °C (S5), respectively. Decreasing the values of these thermal parameters ( $T_g$ ,  $T_c$ , and  $T_m$ ) can be associated with replacing the Bi–O bonds with ones that are less rigid than B–O bonds. On the other hand, R.S. Kundu et al. Found that the  $T_g$  values of glasses in the  $60\text{TeO}_2-x\text{Bi}_2\text{O}_3-(30-x)\text{B}_2\text{O}_3-10\text{ZnO}$  system, where  $0 \leq x \leq 20 \text{ mol\%}$ , decrease as the  $\text{Bi}_2\text{O}_3$  content increases. This decrease in  $T_g$  with bismuth content may be attributed to two possible reasons: firstly, there could be a change in the structure of  $\text{TeO}_2$  in the glass compositions studied here; secondly, the oxygen packing density could be reduced, indicating that the structure becomes more loosely packed. A loosely packed structure requires less internal energy for chain mobility, which is necessary for glass transition. As a result, incorporating  $\text{Bi}_2\text{O}_3$  into the glass framework signifies the creation of more macromolecular chains that are more open in nature. This, in turn, causes a reduction in  $T_g$  [37].

In addition, it can follow the impact of  $\text{Bi}_2\text{O}_3$  on the structural stability of these obtained glasses by determining the parameters  $H_R$  and  $T_{rg}$ , which are calculated by Eqs. (9) and (10):

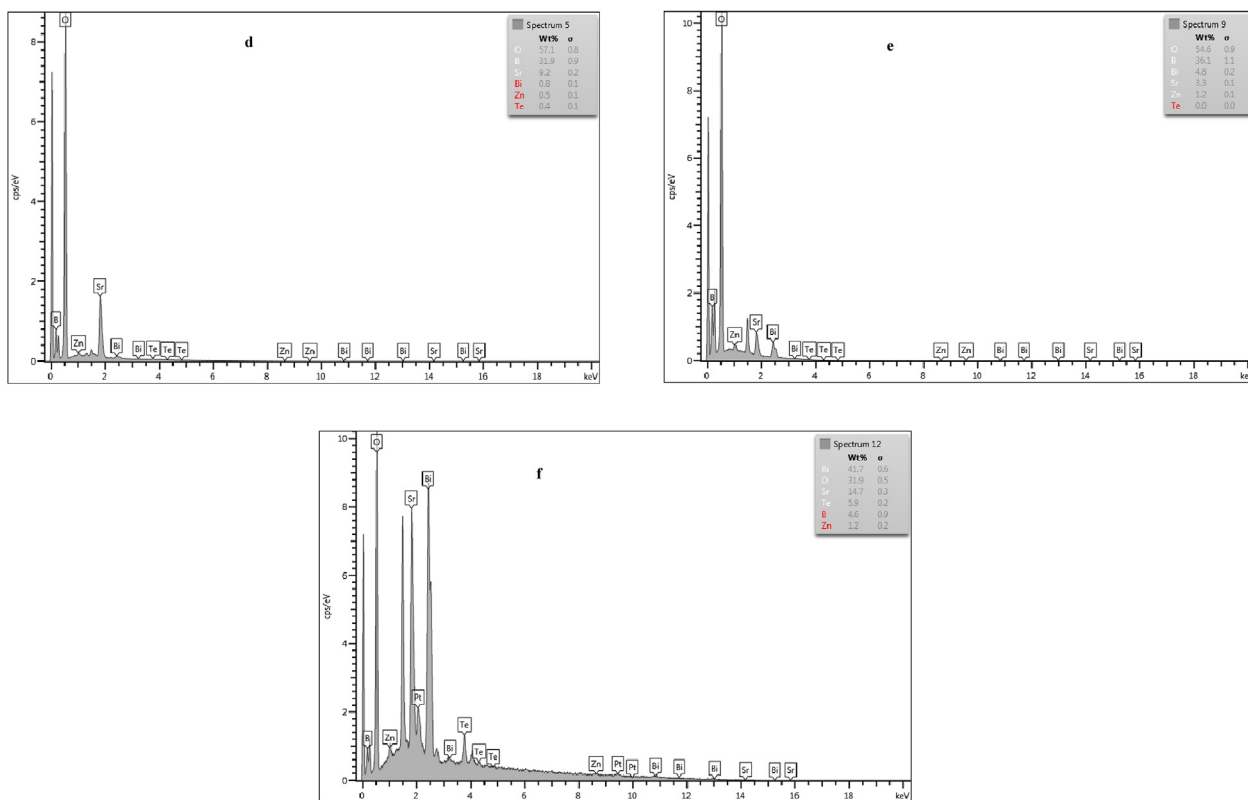


**Fig. 2 – EDX spectra of the glasses S1 (d), S2 (e), and S5 (f).**

$$H_R = \frac{T_c - T_g}{T_m - T_c} \quad (9)$$

$$T_{rg} = \frac{T_g}{T_m} \quad (10)$$

The values corresponding to the calculated parameters,  $H_r$  and  $T_{rg}$ , are summarized in Table 3. Additionally, a variety of methods are used to examine the level of glass stability based on the  $T_g$ ,  $T_c$ , and  $T_m$  characteristic temperatures acquired from DSC curves. Sakka and Mackenzie [36,38], examined the glass thermal stability of several compounds using the ratio  $T_g/T_m$ . Furthermore, the glass criterion [ $T = (T_c - T_g)$ ] is an important measurement that provides information on glass stability and glass production capacity [39]. A more constrained crystallization process is implied by a higher value of  $\Delta T$ . Hruby devised the  $H_r$  criterion,  $H_r = \Delta T/(T_m - T_p)$ , using the aforementioned typical temperatures. Where the value of  $H_r$

provides details on the likelihood of glass formation. According to Fig. 4 and Table 3, the thermal stability parameters ( $\Delta T$  and  $H_R$ ) rise as the  $\text{Bi}_2\text{O}_3$  content rises. Materials with higher values ( $\Delta T$ : from 147.84 °C to 203.69 °C and  $H_R$ : from 0.94 to 1.57) of these factors typically have greater glass thermal stability because they enable the prediction of glass-forming ability. Elsewhere, the parameter  $T_{rg}$  may not explain the stability in this case of these glasses because it varies inversely (from 0.66 to 0.61) with the parameters  $\Delta T$  and  $H_R$  (see Table 3 and Fig. 5). Finally, the calculated parameters' values are affected by the stability ( $\Delta T$  and  $H_R$ ), which increases with increasing  $\text{Bi}_2\text{O}_3$  content in the glassy network [40]. This allows us to use these glasses containing the  $\text{Bi}_2\text{O}_3$  content as good radiation shields (see the next section on the radiation shielding). In addition, the thermal analysis of the obtained glasses could offer good information about their mechanical state (see the mechanical properties section).

**Table 2 – Elemental compositions in glasses S1, S2, and S5 obtained from EDX analyses.**

Element	Atomic number	Atomic weight	S1		S2		S5	
			(Wt.%)	(At.%)	(Wt.%)	(At.%)	(Wt.%)	(At.%)
O	8.00	16.00	57.10	53.75	54.60	49.96	31.94	69.93
B	5.00	10.81	31.90	44.45	36.10	48.89	4.60	14.92
Bi	83.00	208.98	0.80	0.06	4.80	0.34	41.70	7.00
Sr	40.00	87.62	9.20	1.58	3.30	0.55	14.70	5.88
Zn	30.00	65.38	0.50	0.12	1.20	0.27	1.20	0.64
Te	52.00	127.60	0.40	0.05	0.00	0.00	5.90	1.62
<b>Total</b>			99.90	100.00	100.00	100.00	100.00	100.00

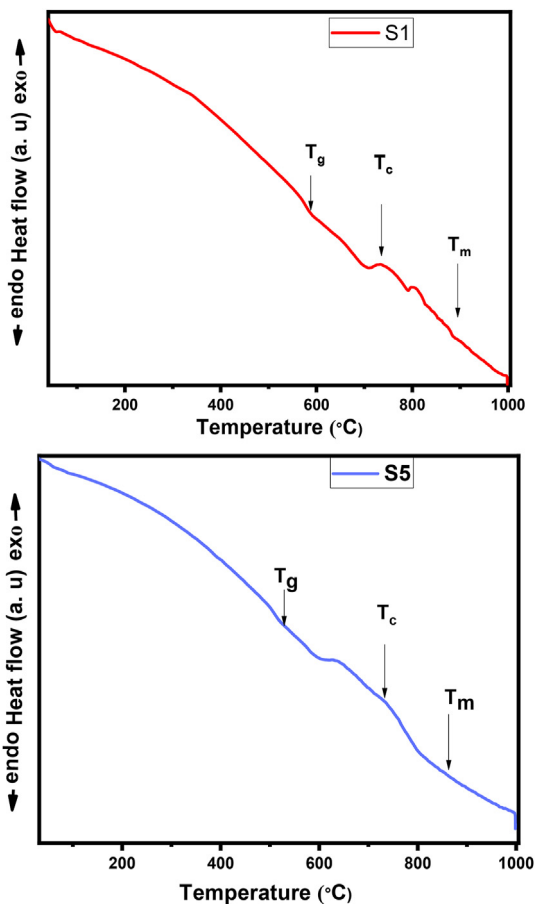


**Fig. 3 – Plots of Differential Thermal Analysis DTA of prepared glasses S1 and S5.**

### 3.3. Mechanical properties

Glass mechanical properties are affected by microstructure and phase crystalline assembly [41]. Glass hardness is commonly interpreted as resistance to abrasion and scratching [42]. Glass properties vary significantly with chemical composition [43]. Microscopic cracks or surface layer defects determine glass strength [44]. Glass has exceptional properties such as high resistance, hardness, and low toughness fracture, which have numerous technological applications in house construction, bridge construction, and medicine (biocompatibility, prosthetic dentistry) [45].

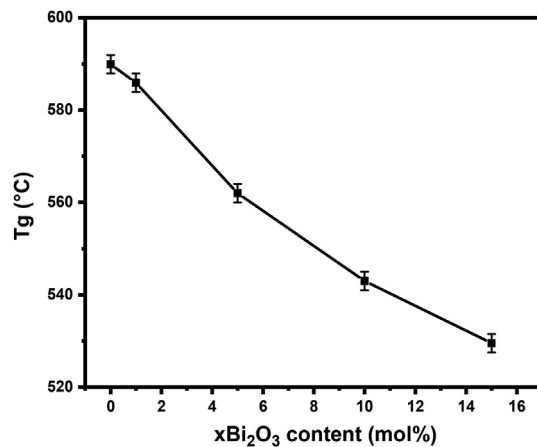


**Fig. 4 – Variation of the glass transition temperature ( $T_g$ ) as a function  $x\text{Bi}_2\text{O}_3$  mol%.**

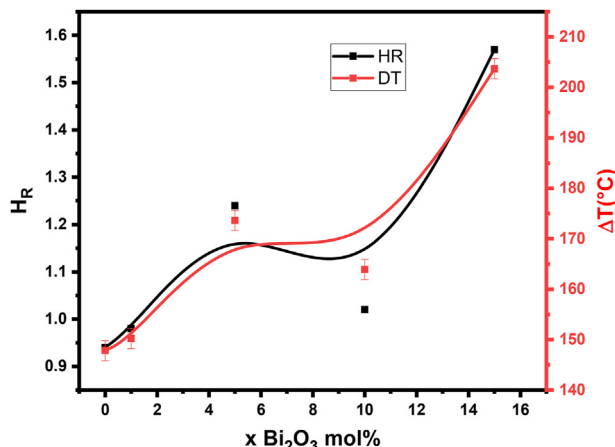


**Fig. 5 – Evolution of the thermal parameters: HR and DT as a function of  $\text{Bi}_2\text{O}_3$  content.**

The pressure needed to remove the vacant space in glass and reflect the glass network's distortion is known as micro-hardness. Glass's free space is reduced by applying high hydrostatic pressure, leading to a denser glass structure [46].

The Vickers hardness does not change linearly with the  $\text{Bi}_2\text{O}_3$  level, as demonstrated in Fig. 6 and Table 4. That is, regardless of the  $\text{Bi}_2\text{O}_3$  composition, the hardness changes significantly while its value remains essentially constant. It is found that the hardness value increased from 2.422 GPa (S1) to 2.989 GPa (S4), then it decreased to 1.420 GPa (S5) as the concentration of  $\text{Bi}_2\text{O}_3$  content increases from 0 (S1) to 15 (S5) mol %. The increase in hardness,  $H_v$ , might be due to change of structural units from  $\text{TeO}_4$  to  $\text{TeO}_3$  with the formation of non-bridging oxygen atoms that results in decreasing of compactness of the glass network. But the decreasing in hardness could be associated to decreasing the formation of non-bridging oxygen atoms [47].

The proportion of transverse to longitudinal strain generated under a tensile force is known as Poisson's ratio. Fig. 7 illustrates the variation of the Poisson's ratio as a function of the  $\text{Bi}_2\text{O}_3$  mol%. As shown in Table 5, with the increase in  $\text{Bi}_2\text{O}_3$

**Table 3 – Determinate thermal parameters ( $T_g$ ,  $T_c$ ,  $T_m$ ,  $H_R$ ,  $T_{rg}$ , and  $\Delta T$ ) of the glasses S1, S2, S3, S4, and S5.**

glasses	S1	S2	S3	S4	S5
parameters					
$T_g \pm 2$ (°C)	589.90	585.90	561.97	542.98	529.51
$T_c \pm 2$ (°C)	737.74	736.11	735.60	706.89	733.20
$T_m \pm 2$ (°C)	895.05	888.50	875.47	868.15	862.56
$H_R$	0.94	0.98	1.24	1.02	1.57
$T_{rg}$	0.66	0.66	0.64	0.62	0.61
$\Delta T \pm 4$ (°C)	147.84	150.21	173.63	163.91	203.69

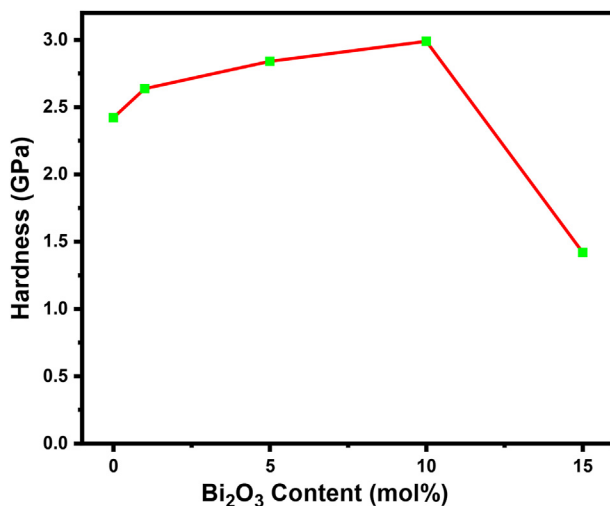


Fig. 6 – Hardness against Bi<sub>2</sub>O<sub>3</sub> content (mol%).

concentration from 0 (S1) to 15 (S5) mol%, Poisson's ratio undergoes a decrease from 0.1684 (S1) to 0.1096 (S2), an increase from 0.1096 (S2) to 0.3204 (S3), and another decrease from 0.3204 (S3) to 0.0973 (S5). Crosslink density is known to impact Poisson's ratio values, indicating whether the glass structure has high or low cross-link density. Furthermore, changes in bonding type from covalent to ionic or vice versa and the average cross-link density of the glass can affect Poisson's ratio values [47–49].

Table 5 presents the longitudinal and shear ultrasonic velocity variations at room temperature for glasses with a composition of (70-x)Bi<sub>2</sub>O<sub>3</sub>–5TeO<sub>2</sub>–20SrO–5ZnO–xBi<sub>2</sub>O<sub>3</sub>, while Fig. 8 provides a visual representation of the data. The longitudinal ultrasonic velocity (V<sub>L</sub>) shows a decreasing trend from 5111.11 m/s (S1) to 5111.11 m/s (S4), while the shear ultrasonic velocity (V<sub>S</sub>) initially increases from 3700.44 m/s (S1) to 3783.78 m/s (S2), followed by a decline to 3305 m/s (S4). However, at the composition S4 (x = 10 mol%), both the longitudinal and shear ultrasonic velocities begin to rise, leading up to the composition S5 (x = 15 mol%). The glass structure experiences a significant change upon the addition of Bi<sub>2</sub>O<sub>3</sub>, which is reflected in the difference in the ultrasonic velocities of the glass network [49]. The reduction in ultrasonic velocities is associated with a decrease in the rigidity of the glass, which is caused by the addition of Bi<sub>2</sub>O<sub>3</sub>, resulting in a shift of structural units from TeO<sub>4</sub> to TeO<sub>3</sub> and the formation of non-bridging oxygen atoms (NBOs), leading to the glass network becoming sparsely packed [46]. Additionally, the decrease in longitudinal and shear ultrasonic velocities may be attributed to the increase in the oxygen molar volume, which causes a weakening of the glass structure [50].

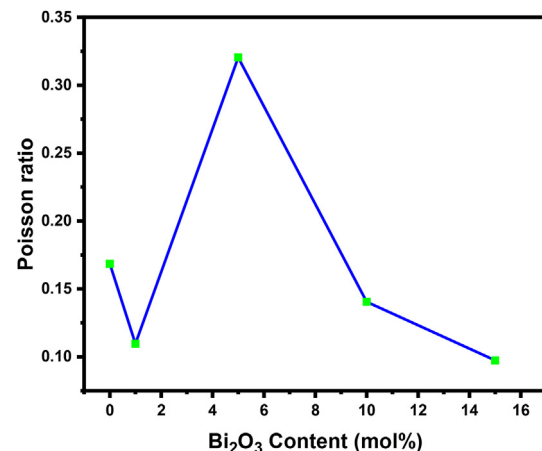


Fig. 7 – Poisson ratio against Bi<sub>2</sub>O<sub>3</sub> content (mol%).

It is advantageous to have a solid understanding of the elastic moduli of glassy materials for the process of drawing glass. Naturally, the elastic moduli of the examined glasses L, G, and E increased in value from 99.58 to 113.06 GPa, 39.71–50.44 GPa, and 92.79–110.69 GPa, respectively, whereas K's elastic moduli decreased from 46.63 to 45.81 GPa. The variation of L, G, E, and K of the current glasses as a function of Bi<sub>2</sub>O<sub>3</sub> concentrations is shown in Fig. 9. The glasses being studied show a variation in their elastic moduli. Specifically, the longitudinal modulus, L, decreases from 99.58 Gpa (S1) to 90.72 Gpa (S3) and then increases to 113.06 Gpa (S5). The shear modulus, G, increases from 39.71 Gpa (S1) to 42.95 GPa (S2), then decreases to 23.97 Gpa (S3), and then increases to 50.44 Gpa (S5). Similarly, the bulk modulus, K, decreases from 46.63 Gpa (S1) to 40.69 GPa (S2), then increases to 58.76 Gpa (S3), and then decreases to 45.81 Gpa (S5). Young's modulus, E, shows an increase from 92.79 to 95.32 GPa (S2), followed by a decrease to 63.30 Gpa (S3), and then an increase to 110.69 Gpa (S5). The changes in elastic moduli can be attributed to the structural unit of the glass changing from TeO<sub>4</sub> to TeO<sub>3</sub> with the formation of non-bridging oxygen atoms. This change in rigidity is responsible for the observed increase or decrease in the elastic moduli of the glass samples. The differences between longitudinal modulus, L, and shear modulus, G, can be attributed to changes in volume due to compressions and expansions that are involved in longitudinal strain, whereas no change in volume occurs in shear strain [46,47,51].

### 3.5. Radiation shielding study

When analyzing the ability of a substance to protect against ionizing radiation, the effective atomic number ( $Z_{\text{eff}}$ ) of the

Table 4 – Vickers hardness of the synthesized glasses system.

Glass sample	Hardness	D1±0.001	D2±0.0013	HV(Gpa)
S1	2004.50 ± 24	0.03	0.031	2.422 ± 0.102
S2	2116.50 ± 19	0.0284	0.0281	2.638 ± 0.122
S3	2126.40 ± 26	0.0258	0.0261	2.840 ± 0.141
S4	2273.77 ± 23	0.0249	0.0248	2.989 ± 0.156
S5	1153.20 ± 35	0.0518	0.0522	1.420 ± 0.035

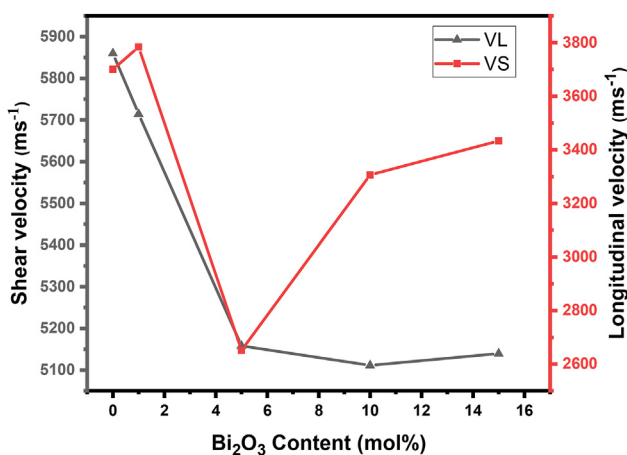
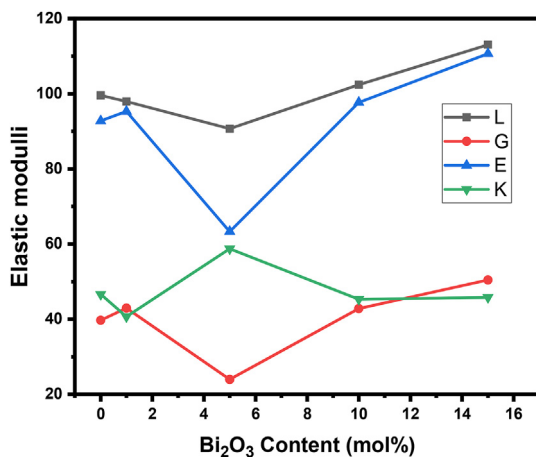
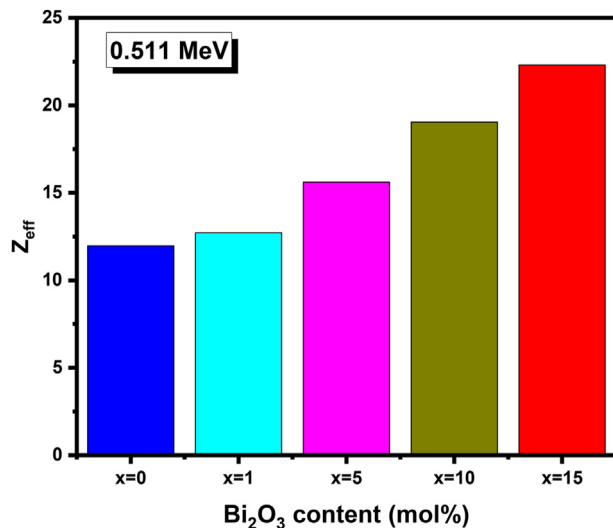
**Table 5 – The Ultrasonic velocities, elastic moduli and poison's ratio in S1–S5 glasses.**

Glass Codes	Ultrasonic velocities		Elastic Moduli			Poison ratio	
	V <sub>L</sub> (m.s <sup>-1</sup> )	V <sub>S</sub> (m.s <sup>-1</sup> )	L GPa	G GPa	E GPa	K Gpa	$\sigma$
S1	5859.87	3700.44	99.58	39.71	92.79	46.63	0.1684
S2	5714.29	3783.78	97.96	42.95	95.32	40.69	0.1096
S3	5157.89	2651.30	90.72	23.97	63.30	58.76	0.3204
S4	5111.11	3305.79	102.40	42.84	97.71	45.29	0.1404
S5	5139.66	3432.84	113.06	50.44	110.69	45.81	0.0973

substance is one of the most important factors to consider. For the prepared glasses, we evaluated the  $Z_{\text{eff}}$  at 0.511 MeV. We used Phy-X software to determine the  $Z_{\text{eff}}$  at this energy [52]. We plotted the  $Z_{\text{eff}}$  for the investigated glasses at 0.511 MeV in Fig. 10. The  $Z_{\text{eff}}$  of the investigated glasses appears to increase as the concentration of  $\text{Bi}_2\text{O}_3$  increases from 0 mol% to 15 mol %. This suggests that the glass with  $x = 15$  mol% has the highest  $Z_{\text{eff}}$ . The reason for this trend is likely due to the higher atomic number of Bi (83) compared to that of B (5), which suggests that the introduction of  $\text{Bi}_2\text{O}_3$  into the glass composition results in an increased average atomic number of the glass network. This increase in  $Z_{\text{eff}}$  may reflect a higher density of

electrons in the glass, resulting in enhanced absorption of radiation at 0.511 MeV, as seen in Fig. 10. Overall, the results suggest that the addition of  $\text{Bi}_2\text{O}_3$  can significantly affect the atomic structure of glasses, which could have important implications for their physical and optical properties. The numerical values of the effective atomic number ( $Z_{\text{eff}}$ ) for the glasses with  $x = 0$  and  $x = 15$  mol% are 11.97 and 22.31, respectively, indicating a significant increase in  $Z_{\text{eff}}$  with increasing concentration of  $\text{Bi}_2\text{O}_3$ . Based on the observed increase in  $Z_{\text{eff}}$  from 0 to 15 mol%, it can be inferred that the  $Z_{\text{eff}}$  will roughly double its initial value if the concentration of  $\text{Bi}_2\text{O}_3$  is further increased from 0 to 30 mol%. The observed increase in  $Z_{\text{eff}}$  may also reflect an increase in electron density in the glass, which could have important implications for the glass's physical and optical properties. This suggests that the  $Z_{\text{eff}}$  glass sample has the potential for enhanced radiation shielding and might be exploited to develop novel radiation shielding glasses.

In Fig. 11, we compared the  $Z_{\text{eff}}$  for these glasses at 0.511 MeV with  $\text{B}_2\text{O}_3$ – $\text{Bi}_2\text{O}_3$ – $\text{PbO}$ – $\text{Al}_2\text{O}_3$ – $\text{CuO}$  glasses [53]. The glasses selected for the comparison in this figure contain 20 mol% of  $\text{Bi}_2\text{O}_3$ . Also, they contained  $\text{PbO}$ , which is a heavy metal oxide. The 20 mol% of  $\text{Bi}_2\text{O}_3$  and the  $\text{PbO}$  can increase the  $Z_{\text{eff}}$  for the  $\text{B}_2\text{O}_3$ – $\text{Bi}_2\text{O}_3$ – $\text{PbO}$ – $\text{Al}_2\text{O}_3$ – $\text{CuO}$  glasses, however, we found that, from our glasses, the sample with 15 mol% of  $\text{Bi}_2\text{O}_3$  has almost the same  $Z_{\text{eff}}$  as the sample with a composition of  $66.5\text{B}_2\text{O}_3$ – $20\text{Bi}_2\text{O}_3$ – $6\text{PbO}$ – $7\text{Al}_2\text{O}_3$ – $0.5\text{CuO}$ .

**Fig. 8 – Shear and longitudinal velocities against  $\text{Bi}_2\text{O}_3$  content (mol%).****Fig. 9 – Elastic moduli variation with  $\text{Bi}_2\text{O}_3$  content (mol%).****Fig. 10 – The effective atomic number of the investigated glasses at 0.511 MeV.**

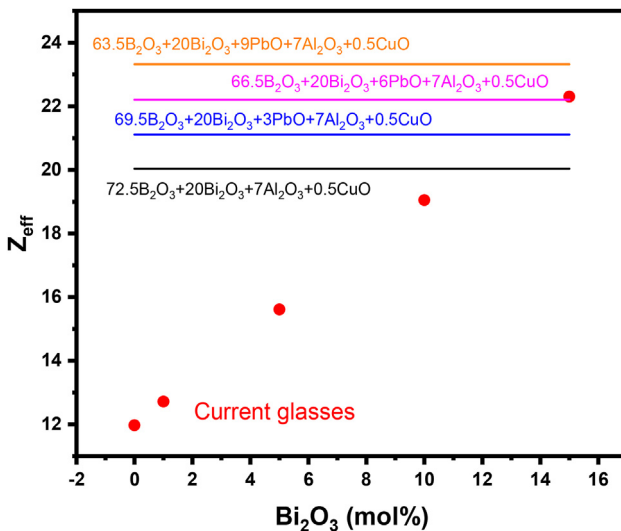


**Fig. 11 – The effective atomic number of the investigated glasses at 0.511 MeV in comparison with  $\text{B}_2\text{O}_3\text{-}\text{Bi}_2\text{O}_3\text{-}\text{PbO}\text{-}\text{Al}_2\text{O}_3\text{-}\text{CuO}$  glasses.**

Also, the  $Z_{\text{eff}}$  for the glass with a composition of  $72.5\text{B}_2\text{O}_3\text{-}20\text{Bi}_2\text{O}_3\text{-}7\text{Al}_2\text{O}_3\text{-}0.5\text{CuO}$  is 20.04, which is close to the  $Z_{\text{eff}}$  for our glass with 15 mol% of  $\text{Bi}_2\text{O}_3$  which is 19.05.

In Fig. 12, we compared our glasses to those of glasses containing high concentrations of  $\text{BaO}$  (40–46 mol%) [54]. By comparing the characteristics of these glasses, we can gain insights into how the addition of  $\text{Bi}_2\text{O}_3$  affects the shielding properties of the glass network. It is well known that  $\text{BaO}$  is a heavy metal oxide and that using it in glasses can result in glasses with relatively high  $Z_{\text{eff}}$ . Among our glasses, the sample with 5 mol% of  $\text{Bi}_2\text{O}_3$  has a close  $Z_{\text{eff}}$  with the glass containing 42 mol% of  $\text{BaO}$  from the  $\text{CaF}_2\text{-}\text{BaO}\text{-}\text{P}_2\text{O}_5$  glass system. Also, from our glasses, the two samples with 0 and

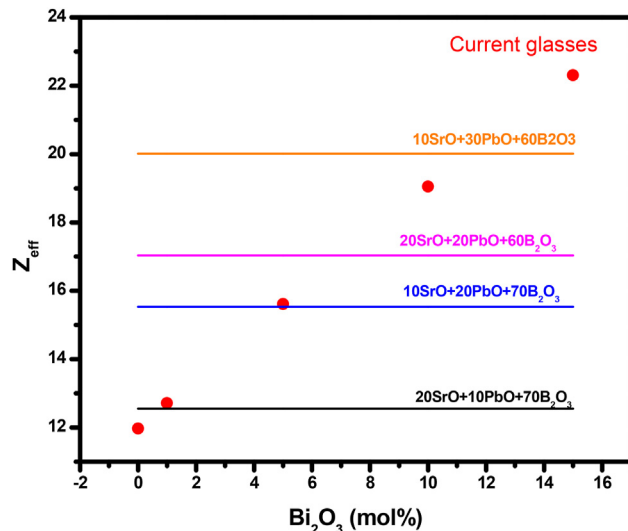


**Fig. 13 – The effective atomic number of the investigated glasses at 0.511 MeV in comparison with  $\text{SrO}\text{-}\text{PbO}\text{-}\text{B}_2\text{O}_3$  glasses.**

1 mol% of  $\text{Bi}_2\text{O}_3$  have a lower  $Z_{\text{eff}}$  than all the  $\text{CaF}_2\text{-}\text{BaO}\text{-}\text{P}_2\text{O}_5$  glasses. However, when we used 10% and 15% mol%  $\text{Bi}_2\text{O}_3$ , we obtained glasses with a higher  $Z_{\text{eff}}$  than the  $\text{CaF}_2\text{-}\text{BaO}\text{-}\text{P}_2\text{O}_5$  glass system. Overall, this analysis helps to place the findings of our investigation into a broader context and highlights the unique properties of our  $\text{Bi}_2\text{O}_3$ -containing glasses.

In Fig. 13, we compared our current glasses in terms of  $Z_{\text{eff}}$  with borate glasses, which contain 10–30 mol% of  $\text{PbO}$  [55]. Our prepared glasses with 0 mol% and 1 mol% of  $\text{Bi}_2\text{O}_3$  showed a close  $Z_{\text{eff}}$  with  $20\text{SrO}\text{-}10\text{PbO}\text{-}70\text{B}_2\text{O}_3$ . Also, our glass sample with 5 mol% shows a close  $Z_{\text{eff}}$  with  $10\text{SrO}\text{-}20\text{PbO}\text{-}70\text{B}_2\text{O}_3$ .  $10\text{SrO}\text{-}20\text{PbO}\text{-}70\text{B}_2\text{O}_3$  glasses contain 20 mol% of  $\text{PbO}$  (which is a toxic compound). From our glasses, the glass with 5 mol%

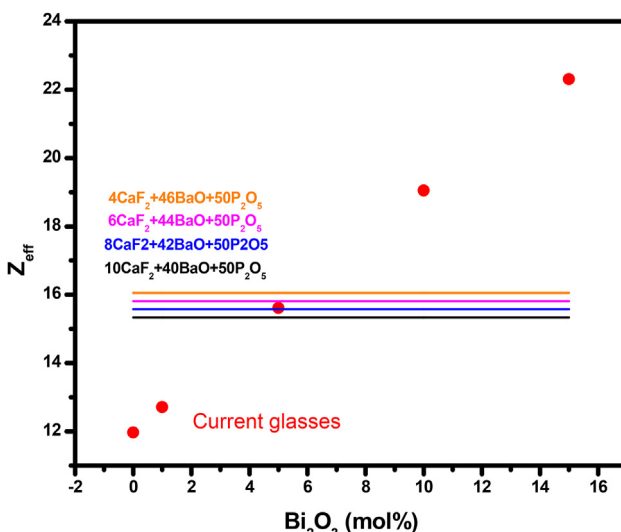


**Fig. 12 – The effective atomic number of the investigated glasses at 0.511 MeV in comparison with  $\text{CaF}_2\text{-}\text{BaO}\text{-}\text{P}_2\text{O}_5$  glasses.**

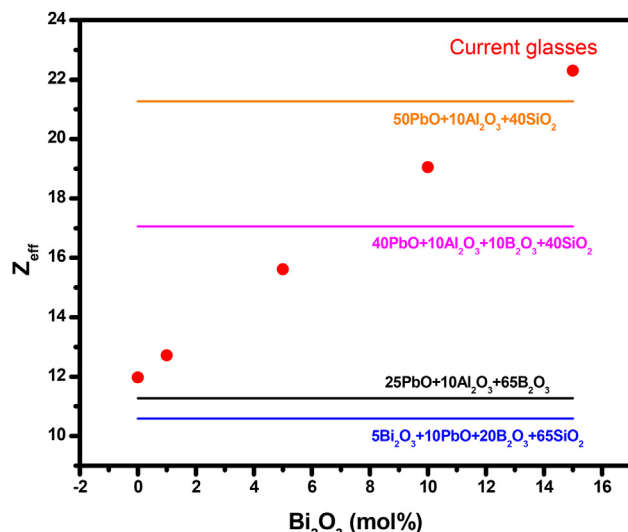


**Fig. 14 – The effective atomic number of the investigated glasses at 0.511 MeV in comparison with glasses containing  $\text{Bi}_2\text{O}_3$  and  $\text{PbO}$ .**

of  $\text{Bi}_2\text{O}_3$  has the same  $Z_{\text{eff}}$  as the glass with 20 mol% of  $\text{PbO}$ . So, we can use a glass sample with the same effectiveness in radiation protection but containing  $\text{Bi}_2\text{O}_3$  instead of  $\text{PbO}$ , so we can reduce the environmental issues of the lead. On the other hand, the same degree of radiation safety efficiency can be obtained while lowering the possible environmental impact of lead by substituting  $\text{Bi}_2\text{O}_3$  for  $\text{PbO}$  in the glass composition. Radiation shielding can be accomplished in a way that is less harmful to the environment if  $\text{Bi}_2\text{O}_3$  is used rather than lead oxide.

In Fig. 14, we showed the comparison between the  $Z_{\text{eff}}$  for our glasses and that other glasses containing  $\text{Bi}_2\text{O}_3$  and  $\text{PbO}$  [56]. All of our glasses showed better radiation shielding properties than  $25\text{PbO}-10\text{Al}_2\text{O}_3-65\text{B}_2\text{O}_3$  and  $5\text{Bi}_2\text{O}_3-10\text{PbO}-20\text{B}_2\text{O}_3-65\text{SiO}_2$  glasses. Among our samples, the glass with 10 mol%  $\text{Bi}_2\text{O}_3$  showed a higher  $Z_{\text{eff}}$  than  $40\text{PbO}-10\text{Al}_2\text{O}_3-10\text{B}_2\text{O}_3-40\text{SiO}_2$ . Also, the glass in this investigation containing 10 mol% of  $\text{Bi}_2\text{O}_3$  showed higher  $Z_{\text{eff}}$  than  $50\text{PbO}-10\text{Al}_2\text{O}_3-40\text{SiO}_2$ .

#### 4. Conclusion

Bismuth-doped telluro-borate glasses were synthesized to study their structural, thermal, mechanical, and radiation-shielding properties. The morphology studies confirmed the amorphous state by showing no agglomeration on the glassy surfaces. The glass transition temperature ( $T_g$ ) was found to decrease from 589.90 °C to 529.51 °C with increasing the  $\text{Bi}_2\text{O}_3$  content from 0 mol% to 15 mol% as a result of the  $\text{Bi}-\text{O}$  bonds ( $\Delta H_{f298} = 343 \text{ Kj/mol}$ ) replacing  $\text{B}-\text{O}$  bonds ( $\Delta H_{f298} = 806 \text{ Kj/mol}$ ). The mechanical parameters, like the Vickers hardness, the longitudinal modulus ( $L$ ), the shear modulus ( $S$ ), the Young's modulus ( $\epsilon$ ), and the bulk modulus ( $K$ ), have been evaluated for studying the influence of the  $\text{Bi}_2\text{O}_3$  content on the mechanical properties of present glasses. The ultrasonic velocities decreased as the concentration of  $\text{Bi}_2\text{O}_3$  increased. The Phy-X software was used to evaluate the radiation properties of the current glasses. We compared the  $Z_{\text{eff}}$  in the current glasses with those in other glasses containing different HMOs. From the comparisons, we reached the conclusion that we can use a glass sample with the same effectiveness in radiation protection but containing  $\text{Bi}_2\text{O}_3$  instead of  $\text{PbO}$ , so we can reduce the environmental issues of the lead.

#### Declaration of Competing Interest

The authors declare that they have no known competing financial interests or personal relationships that could have appeared to influence the work reported in this paper.

#### Acknowledgments

This work was supported by UTM-Professional Development Research University (POST DOCTORAL FELLOWSHIP Ref No: PY/2022/03183) and FRGS grant (vot num: R.J130000.7854.5F236, Ref No: PY/2019/01269).

#### REFERENCES

- [1] ElBatal F, Marzouk M, Abdel Ghany A. Gamma rays interaction with bismuth borate glasses doped by transition metal ions. *J Mater Sci* 2011;46:5140–52.
- [2] Rammah Y, Ali A, El-Mallawany R, Abdelghany A. Optical properties of bismuth borotellurite glasses doped with  $\text{NdCl}_3$ . *J Mol Struct* 2019;1175:504.
- [3] Thabit HA, Kabir NA, Al Mutairi AM, Bafaqeer A, Alraddadi S, Jaji N-D, et al. Investigation of the thermoluminescence dosimeter characteristics of multilayer  $\text{ZnO}$  (300 nm)/Ag (50 nm)/ $\text{ZnO}$  (x) thin films for photonic dosimetry applications. *Optic Mater* 2023;137:113548.
- [4] Fidan M, Acikgoz A, Demircan G, Yilmaz D, Aktas B. Optical, structural, physical, and nuclear shielding properties, and albedo parameters of  $\text{TeO}_2-\text{BaO}-\text{B}_2\text{O}_3-\text{PbO}-\text{V}_2\text{O}_5$  glasses. *J Phys Chem Solid* 2022;163:110543.
- [5] Aktas B, Acikgoz A, Yilmaz D, Yalcin S, Dogru K, Yorulmaz N. The role of  $\text{TeO}_2$  insertion on the radiation shielding, structural and physical properties of borosilicate glasses. *J Nucl Mater* 2022;563:153619.
- [6] Geidam I, Matori K, Halimah M, Chan K, Muhammad F, Ishak M, et al. Oxide ion polarizabilities and gamma radiation shielding features of  $\text{TeO}_2-\text{B}_2\text{O}_3-\text{SiO}_2$  glasses containing  $\text{Bi}_2\text{O}_3$  using Phy-X/PSD software. *Mater Today Commun* 2022;31:103472.
- [7] Zubair M, Ahmed E, Hartanto D. Comparison of different glass materials to protect the operators from gamma-rays in the PET using MCNP code. *Radiat Phys Chem* 2022;190:109818.
- [8] Acikgoz A, Demircan G, Yilmaz D, Aktas B, Yalcin S, Yorulmaz N. Structural, mechanical, radiation shielding properties and albedo parameters of alumina borate glasses: Role of  $\text{CeO}_2$  and  $\text{Er}_2\text{O}_3$ . *Mater Sci Eng B* 2022;276:115519.
- [9] Bagheri R, Khorrami Moghaddam A, Yousefnia H. Gamma ray shielding study of barium–bismuth–borosilicate glasses as transparent shielding materials using MCNP-4C code, XCOM program, and available experimental data. *Nucl Eng Technol* 2017;49(1):216–23.
- [10] Chaiphaksa W, Borisut P, Chanthima N, Kaewkhae J, Sanwaranatee N. Mathematical calculation of gamma rays interaction in bismuth gadolinium silicate glass using WinXCom program. *Mater Today Proc* 2022;65:2412.
- [11] Bhattoo R, Bishnoi S, Zaki M, Krishnan NA. Understanding the compositional control on electrical, mechanical, optical, and physical properties of inorganic glasses with interpretable machine learning. *Acta Mater* 2023;242:118439.
- [12] Linganna K, Ju S, Ryu Y, Naeem K, Jeong H, Kim BH. Effect of  $\text{WO}_3$  on physical and magneto-optical properties of  $\text{TeO}_2-\text{La}_2\text{O}_3-\text{WO}_3$  glasses for magneto-optics application. *Result Phys* 2022;43:106069.
- [13] Baach B, Ferraa S, Barebita H, Nimour A, Guedira T. Effect of alkaline-earth metal oxides on physical properties and structure of bismuth–vanadate glasses. *Inorg Chem Commun* 2022;146:110076.
- [14] Thabit HA, Ismail AK, Jagannath G, I. A, Hashim S, Sayyed MI. Physical, optical and spectroscopic characteristics investigation for doped  $\text{Dy}^{3+}$  borate glass matrix. *J Non-Cryst Solid* 2023;608:122258.
- [15] Chanakya N, Madhuri JH, Devi CS, Prasad M, Jagadeshwar V, Upender G. Effect of  $\text{B}_2\text{O}_3$  and  $\text{Li}_2\text{O}$  on vibrational, thermal and optical properties of  $50\text{Bi}_2\text{O}_3-15\text{PbO}-(35-x)\text{B}_2\text{O}_3-x\text{Li}_2\text{O}$  ( $0 \leq x \leq 25$  mol%) glasses. *Optik* 2022;271:170109.
- [16] de Oliveira Lima AM, de Queiroz MN, dos Santos Bianchi G, Astrath NG, Pedrochi F, Steimacher A, et al. Structural and thermal properties of  $\text{Yb}:\text{CaBTeX}$  glasses as a function of  $\text{TeO}_2$  content. *J Non-Cryst Solid* 2022;595:121848.
- [17] Wang Z, Lin X, Liu T, Liu L, Jiang X, Yu Y, et al. Thermal, chemical properties and structure evolution of medical

- neutral glasses modified by transition metal oxides. *J Non-Cryst Solid* 2022;595:121835.
- [18] EL-Kameesy S, Thabit: Radionuclides Concentrations in Some Rock Samples Used as Building Material from Yafea Area in Yemen. *Arab J Nucl Sci Appl* 2016;49(1):46.
- [19] Thabit HA, Kabir NA. The study of X-ray effect on structural, morphology and optical properties of ZnO nanopowder. *Nucl Instr Method Phys Res Sect B Beam Interact Mater Atom* 2018;436:278.
- [20] Mama Touloou MB, Fossati PCM, Rountree CL. Systematic approach to thermophysical and mechanical properties of SiO<sub>2</sub>–B<sub>2</sub>O<sub>3</sub>–Na<sub>2</sub>O glasses using molecular dynamics simulations. *J Non-Cryst Solids* 2023;603:122099.
- [21] Zhang S, Wei C, Shi Z, Zhang H, Ma M. Effect of Fe addition on the glass-forming ability, stability, and mechanical properties of Zr<sub>50</sub>Cu<sub>34</sub>-xFe<sub>x</sub>Al<sub>8</sub>Ag<sub>8</sub> metallic glasses. *J Alloy Compound* 2022;929:167334.
- [22] Zhai C, Zhong Y, Wang M, Zhang J, Zhao Y, Zhu Y. Stabilizing the pore structures of foam glasses for improving the mechanical and physical properties at a low sintering temperature. *Mater Chem Phys* 2022;290:126520.
- [23] Sayyed M, Prabhu NS, Jecong J, Kamath SD. Radiation shielding analysis using EPICS2017 and mechanical property characterization of zinc boro-tellurite alumina glasses. *Optik* 2022;257:168814.
- [24] Kaur P, Singh J, Kaur P, Singh T. Radiation shielding and sensing properties for some Eu<sup>3+</sup> doped bismo-phosphate glasses. *Radiat Phys Chem* 2023;110769.
- [25] Kaewjaeng S, Kothon S, Wantana N, Kim H, Rajaramakrishna R, Jumpee C, et al. Fabrication luminescence and radiation shielding properties of Gd<sub>2</sub>O<sub>3</sub>–La<sub>2</sub>O<sub>3</sub>–ZnO–B<sub>2</sub>O<sub>3</sub>–Sm<sub>2</sub>O<sub>3</sub> glasses. *Radiat Phys Chem* 2023;202:110537.
- [26] Thabit HA, Kabir NA, Ismail AK, Alraddadi S, Bafaqeer A, Saleh MA. Development of Ag-doped ZnO thin films and thermoluminescence (TLD) characteristics for radiation. *Technol Nanomater* 2022;12(17):3068.
- [27] Thabit HA, Kabir NA, Ahmed NM, Alraddadi S, Al-Buraihi MS. Synthesis, structural, optical, and thermoluminescence properties of ZnO/Ag/Y nanopowders for electronic and dosimetry applications. *Ceram Int* 2021;47(3):4249.
- [28] Thabit HA, Ismail AK, Yusof NN, Sayyed MI, Mahmoud KG, Abdullahi I, et al. A closer look at the structure and gamma-ray shielding properties of newly designed boro-tellurite glasses reinforced by bismuth (III) oxide. *Nucl Eng Technol* 2023;55(5):1734.
- [29] Marzouk Y, Xiu D. A stochastic collocation approach to Bayesian inference in inverse problems. 2009.
- [30] Bulus I, Hussin R, Ghoshal S, Tamuri AR, Jupri S. Enhanced elastic and optical attributes of boro-telluro-dolomite glasses: Role of CeO<sub>2</sub> doping. *Ceram Int* 2019;45(15):18648.
- [31] Damas P, Coelho J, Hungerford G, Hussain NS. Structural studies of lithium boro tellurite glasses doped with praseodymium and samarium oxides. *Mater Res Bull* 2012;47(11):3489.
- [32] Divina R, Marimuthu K, Mahmoud K, Sayyed M. Physical and structural effect of modifiers on dysprosium ions incorporated boro-tellurite glasses for radiation shielding purposes. *Ceram Int* 2020;46(11):17929.
- [33] Sava BA, Boroica L, Elisa M, Shikimaka O, Grabco D, Popa M, et al. Bismuth and lead oxides codoped boron phosphate glasses for Faraday rotators. *Ceram Int* 2018;44(6):6016.
- [34] Barik SK, Senapati A, Balakrishnan S, Ananthasivan K. Synthesis and characterization of rare-earth doped aluminium phosphate glasses. *Prog Nucl Energy* 2022;152:104372.
- [35] Es-Soufi H, Bih L, Manoun B, Lazor P. Structure, thermal analysis and optical properties of lithium tungsten-titanophosphate glasses. *J Non-Cryst Solid* 2017;463:12.
- [36] Cottrell TL. The strengths of chemical bonds. Butterworths Scientific Publications; 1958.
- [37] Kundu R, Dhankhar S, Punia R, Nanda K, Kishore N. Bismuth modified physical, structural and optical properties of mid-IR transparent zinc boro-tellurite glasses. *J Alloy Compound* 2014;587:66.
- [38] Sakka S, Mackenzie J. Relation between apparent glass transition temperature and liquids temperature for inorganic glasses. *J Non-Cryst Solids* 1971;6(2):145–62.
- [39] Dahshan A. Thermal stability and crystallization kinetics of new As–Ge–Se–Sb glasses. *J Non-Cryst Solids* 2008;354(26):3034–9.
- [40] Abbady G, Abd-Elnaiem AM. Thermal stability and crystallization kinetics of Ge<sub>13</sub>In<sub>8</sub>Se<sub>79</sub> chalcogenide glass. *Phase Transitions* 2019;92(7):667–82.
- [41] Luo G, Li W, Liang W, Liu G, Ma Y, Niu Y, et al. Coupling effects of glass fiber treatment and matrix modification on the interfacial microstructures and the enhanced mechanical properties of glass fiber/polypropylene composites. *Compos Part B Eng* 2017;111:190.
- [42] Al-Amri A, Evans J. Degradation of the strength of glass after light contact with other materials. *Mater Sci Eng, A* 1994;177(1–2):11–8.
- [43] Yamusa Y, et al. Impact of Eu<sup>3+</sup> on the luminescent, physical and optical properties of BaSO<sub>4</sub>–B<sub>2</sub>O<sub>3</sub>–P<sub>2</sub>O<sub>5</sub> glasses. *Optik* 2018;164:324–34.
- [44] Laopaiboon R, Bootjomchai C. Characterization of elastic and structural properties of alkali-borosilicate glasses doped with vanadium oxide using ultrasonic technique. *Glass Phys Chem* 2015;41:352–8.
- [45] Sawamura S, Wondraczek L. Scratch hardness of glass. *Physical Review Materials* 2018;2(9):092601.
- [46] Halimah M, Daud W, Sidek H. Elastic properties of TeO<sub>2</sub>–B<sub>2</sub>O<sub>3</sub>–Ag<sub>2</sub>O glasses. *Ionics* 2010;16:807–13.
- [47] Eevon C, Halimah M, Azmi Z, Azurahanim C. Elastic properties of TeO<sub>2</sub>–B<sub>2</sub>O<sub>3</sub>–ZnO–Gd<sub>2</sub>O<sub>3</sub> glasses using non-destructive ultrasonic technique. *Chalcogenide Lett* 2016;13(6):281.
- [48] Gaafar M, Shaarany I, Alharbi T. Structural investigations on some cadmium-borotellurate glasses using ultrasonic, FT-IR and X-ray techniques. *J Alloys Compd* 2014;616:625–32.
- [49] Saddeek YB. Elastic properties of Gd<sup>3+</sup>-doped tellurovanadate glasses using pulse-echo technique. *Mater Chem Phys* 2005;91(1):146–53.
- [50] Saddeek YB, Abd El Latif L. Effect of TeO<sub>2</sub> on the elastic moduli of sodium borate glasses. *Phys B Condens Matter* 2004;348(1–4):475–84.
- [51] El-Mallawany R, El-Khoshkhany N, Afifi H. Ultrasonic studies of (TeO<sub>2</sub>)<sub>50</sub>–(V<sub>2</sub>O<sub>5</sub>)<sub>50</sub>–x(TiO<sub>2</sub>)<sub>x</sub> glasses. *Mater Chem Phys* 2006;95(2–3):321–7.
- [52] Şakar E, Özpolat ÖF, Alım B, Sayyed M, Kurudirek M. Phy-X/PSD: development of a user friendly online software for calculation of parameters relevant to radiation shielding and dosimetry. *Radiat Phys Chem* 2020;166:108496.
- [53] Showahy A, Elsamani R, Issa SA, El-Denglawey A, Saddeek YB. Effect of PbO on the elastic and radiation shielding properties of B<sub>2</sub>O<sub>3</sub>–Bi<sub>2</sub>O<sub>3</sub>–Al<sub>2</sub>O<sub>3</sub>–CuO glasses. *Radiat Phys Chem* 2022;196:110129.
- [54] Al-Hadeethi Y, Sayyed M. Evaluation of gamma ray shielding characteristics of CaF<sub>2</sub>–BaO–P<sub>2</sub>O<sub>5</sub> glass system using Phy-X/PSD computer program. *Prog Nucl Energy* 2020;126:103397.
- [55] Kaundal R, Kaur S, Singh N, Singh K. Investigation of structural properties of lead strontium borate glasses for gamma-ray shielding applications. *J Phys Chem Solid* 2010;71(9):1191.
- [56] Sayyed M, Zaid MHM, Effendy N, Matori KA, Lacomme E, Mahmoud K, et al. The influence of PbO and Bi<sub>2</sub>O<sub>3</sub> on the radiation shielding and elastic features for different glasses. *J Mater Res Technol* 2020;9(4):8429.